ADVANCED MATERIALS
www.advmat.de

A Flash-Induced Robust Cu Electrode on Glass Substrates and Its Application for Thin-Film µLEDs

*Jung Ho Shin, Jung Hwan Park, Jeongmin Seo, Tae Hong Im, Jong Chan Kim, Han Eol Lee, Do Hyun Kim, Kie Young Woo, Hu Young Jeong, Yong-Hoon Cho, Taek-Soo Kim, Il-Suk Kang, and Keon Jae Lee**

A robust Cu conductor on a glass substrate for thin-film µLEDs using the flash-induced chemical/physical interlocking between Cu and glass is reported. During millisecond light irradiation, CuO nanoparticles (NPs) on the display substrate are transformed into a conductive Cu film by reduction and sintering. At the same time, intensive heating at the boundary of CuO NPs and glass chemically induces the formation of an ultrathin Cu_2O interlayer within the Cu/glass interface for strong adhesion. Cu nanointerlocking occurs by transient glass softening and interface fluctuation to increase the contact area. Owing to these flash-induced interfacial interactions, the flash-activated Cu electrode exhibits an adhesion energy of 10 J m^{-2}, which is five times higher than that of vacuum-deposited Cu. An AlGaInP thin-film vertical µLED (VLED) forms an electrical interconnection with the flash-induced Cu electrode via an ACF bonding process, resulting in a high optical power density of 41 mW mm^{-2}. The Cu conductor enables reliable VLED operation regardless of harsh thermal stress and moisture infiltration under a high-temperature storage test, temperature humidity test, and thermal shock test. 50 × 50 VLED arrays transferred onto the flash-induced robust Cu electrode show high illumination yield and uniform distribution of forward voltage, peak wavelength, and device temperature.

Inorganic-based micro-light-emitting diodes (µLEDs) have attracted significant attention for next-generation displays that can replace conventional organic light-emitting diodes (OLEDs) and liquid crystal displays (LCDs) because of their fast response time, high power efficiency, and outstanding stability.[1] µLED displays based on individual chip transfer have already been demonstrated in a 150 inch commercial TV on the Consumer Electronics Show (CES) 2020. However, due to the time-consuming and expensive process of multimillion individual chip transfer for UHD TV, chip-based µLED has limitation in the mass production of low-cost µLED displays. In contrast, thin-film µLED based on mass transfer of more than 10 000 LED chips in one time has great potential to reduce the product price of µLED panels.[1–4] Although many innovative studies of thin-film µLED technologies have been performed, little effort has been devoted to the fundamental materials in µLED devices and their effect on performance, reliability, and adhesion control.

Material issues with thin-film µLED are related to the epitaxial wafer, target substrate, electrode, transfer, and packaging.[3,5–19] Glass is currently one of the most widely used display substrates for TVs, smart phones, and tablet PCs.[20–23] Electrode materials for thin-film µLEDs on a glass substrate need to be carefully optimized to improve RC delay, power efficiency, stability, and production cost. Cu is an attractive material for thin-film µLED electrodes due to its remarkable conductivity (5.98×10^5 S cm^{-1}),[24] high robustness,[25,26] and cheap price (≈6500 times cheaper than Au),[27]

J. H. Shin, T. H. Im, Dr. H. E. Lee, Dr. D. H. Kim, Prof. K. J. Lee
Department of Materials Science and Engineering
Korea Advanced Institute of Science and Technology (KAIST)
291 Daehak-ro, Yuseong-gu, Daejeon 34141, Republic of Korea
E-mail: keonlee@kaist.ac.kr
Prof. J. H. Park
Department of Mechanical Engineering (Department of Aeronautics, Mechanical and Electronic Convergence Engineering)
Kumoh National Institute of Technology
61 Daehak-ro, Gumi, Gyeongbuk 39177, Republic of Korea
Dr. J. Seo, Prof. T.-S. Kim
Department of Mechanical Engineering
Korea Advanced Institute of Science and Technology (KAIST)
291 Daehak-ro, Yuseong-gu, Daejeon 34141, Republic of Korea
The ORCID identification number(s) for the author(s) of this article can be found under https://doi.org/10.1002/adma.202007186.
J. C. Kim, Prof. H. Y. Jeong
UNIST Central Research Facilities (UCRF) and
School of Materials Science and Engineering
Ulsan National Institute of Science and Technology (UNIST)
Ulsan 44919, Republic of Korea
K. Y. Woo, Prof. Y.-H. Cho
Department of Physics
Korea Advanced Institute of Science and Technology (KAIST)
291 Daehak-ro, Yuseong-gu, Daejeon 34141, Republic of Korea
Dr. I.-S. Kang
National Nanofab Center
Korea Advanced Institute of Science and Technology (KAIST)
291, Daehak-ro, Yuseong-gu, Daejeon 34141, Republic of Korea

DOI: 10.1002/adma.202007186

as proven by the industrial application of copper interconnects in a-Si TFT-LCD.[28–30] Nonetheless, poor Cu adhesion on glass substrates induces the electrode delamination under minor environmental stresses of temperature and humidity, leading to the breakdown of current-driven μLEDs.[28,29,31] Metal interlayers such as Mo, Cr, and Ti at Cu/glass interface have been proposed; however, they possess a drawback of galvanic reaction during the wet etching process, causing the damage and disconnection of metal lines.[31–33] To solve the inherent atomic mismatch, chemical and physical reactions at the interface between Cu/glass should be investigated.

Light–material interactions have been spotlighted for the surface chemistry of interface via nonequilibrium reactions within extremely short time and focused layer.[34–46] Spatiotemporally controlled photoresponse at the boundary of heterogeneous materials has demonstrated remarkable interface innovations, including nanointerlocking and phase separation that cannot be obtained by traditional thermal annealing.[47–52] From a view point of cost-effectiveness, xenon flash lamps with μs–ms illumination have been exploited to replace industrial excimer lasers in mass production, because of their broad light spectrum, large scalability, and high compatibility to roll process.[44,49,53] Our group reported a flash-induced stretchable Cu conductor with outstanding adhesion to polymer substrates via multiscale interfacial interlocking.[54] To take advantage of flash light sources for display substrates, transient photothermal reactions near the glass transition temperature of ≈600 °C should be employed for physical interlocking, electrode deterioration, and interface-limited chemistry.

Herein, we report a highly robust Cu electrode on a glass substrate for AlGaInP thin-film μLEDs via flash-induced interfacial chemistry and physical interlocking. By millisecond flash-material interactions, the CuO nanoparticles (NPs) were photoreduced to conductive Cu. Simultaneously, a Cu_2O interlayer was formed between the glass and Cu electrode by chemical reaction for strong adhesion interface, as confirmed by scanning transmission electron microscopy (STEM) and Raman spectroscopy. Finite element analysis (FEA) simulations verified that intensive photoheating was focused at the interface between CuO and substrate, due to the low thermal conductivity of glass, resulted in the formation of Cu_2O interlayer. In addition, flash-induced physical interlocking of the Cu electrode to the display substrates was achieved by glass softening and subsequent nanoscale roughening of the Cu/glass interface without oxidation and ablation of the upper electrode. A quantitative double-cantilever beam (DCB) peel test was conducted to measure the adhesion energy of photosintered Cu on glass, and it was found to be five times higher than that of vacuum-deposited Cu. An AlGaInP thin-film vertical μLED (VLED) was electrically interconnected to a flash-induced Cu electrode using Au/Ni coated particles, exhibiting a high optical power density of 41 mW mm^{-2}. The environmental stability of μLED and flash-activated Cu was evaluated by reliability examinations such as the high-temperature storage test, temperature humidity test, and thermal shock test. 50 × 50 thin-film VLED arrays with an average luminescence of 331 cd m^{-2} were demonstrated with uniform distribution of forward voltage, peak wavelength, and device temperature. Robust AlGaInP VLEDs on the glass substrate confirmed the feasibility of flash-induced Cu electrodes for thin-film μLED displays.

Figure 1a schematically illustrates the overall concept of flash-induced robust Cu electrode and its application to AlGaInP thin-film VLEDs. The following is a detailed explanation: i) CuO NPs spin-coated on a glass substrate (Corning Lotus Display Glass) were transformed into a continuous Cu film upon flash light irradiation, inducing successive photothermo-chemical reactions including sintering and deoxidization. Simultaneously, two types of flash-induced interfacial interactions (chemical and physical interlocking) occurred due to intensive heating between the CuO NP layer and glass, resulted in a durable Cu conductor on a glass substrate. The photochemical interfacial reaction successfully formed an extremely thin Cu_2O interlayer within the constrained Cu/glass interface, resolving the inherent atomic lattice mismatch. Physical interlocking of the photoreduced Cu/glass interface was induced through transient glass softening and subsequent interface roughening, increasing the contact area between Cu electrode and substrate. ii) Flash-processed Cu conductors patterned with microscale resolution were electrically interconnected to a 50 × 50 array of thin-film μLEDs using a one-step transfer via an anisotropic conductive film (ACF). The outstanding robustness of Cu electrode allowed stable VLED operation without electrical/optical degradation, despite of severe thermal stress and moisture infiltration.

Figure 1b shows the flash-induced temperature distribution of CuO NPs on a glass substrate, calculated by finite element analysis (FEA), to investigate the theoretical feasibility of interface chemical reaction via the spatiotemporally controlled photothermal effect. The FEA simulation was performed based on optimized processing conditions of 14.45 J cm^{-2} energy density and 3.6 ms pulse width for the Cu conductor with 5.6 μΩ cm resistivity (Figure S1, Supporting Information). The temperature of CuO NPs and substrate under flash light irradiation was determined using the following heat flux equation, Equation (1)[55,56]

$$Q = \rho C \frac{\partial T}{\partial t} + \rho C \cdot \nabla T - \nabla \cdot (k \nabla T) \tag{1}$$

where Q is the thermal energy caused by the flash light and C, ρ, and k are the heat capacity, density, and thermal conductivity of CuO and glass, respectively. Photon energy incident on the CuO NPs was converted to heat, and sequentially accumulated at the interface between CuO NPs and substrate due to the low thermal conductivity of glass (k_{glass} = 0.8 W m^{-1} K^{-1}).[57,58] The intensive photothermal heating of 3.6 ms illumination drastically increased the temperature of CuO/glass interface, up to 930 K, selectively inducing chemical interactions to form an intermediate functional layer.[59] Figure 1c shows the Raman spectrum results of pristine CuO film (before flash), flash-processed Cu conductor (after flash), and residual Cu_2O film (after flash-induced Cu etching) to confirm the interface layers formed by photochemical reaction. The Raman spectrum of pristine CuO film (blue line) exhibited only copper (II) oxide peaks at 293, 343, and 626 cm^{-1}.[60,61] The flash-activated Cu conductor showed no characteristic Raman spectra, due to the presence of free electrons hindering the light–metal interactions, as indicated by the green line.[62,63] For the Cu-removed sample (red line), prominent peaks of copper (I) oxide (Cu_2O), and glass were exhibited, indicating that a Cu_2O layer was

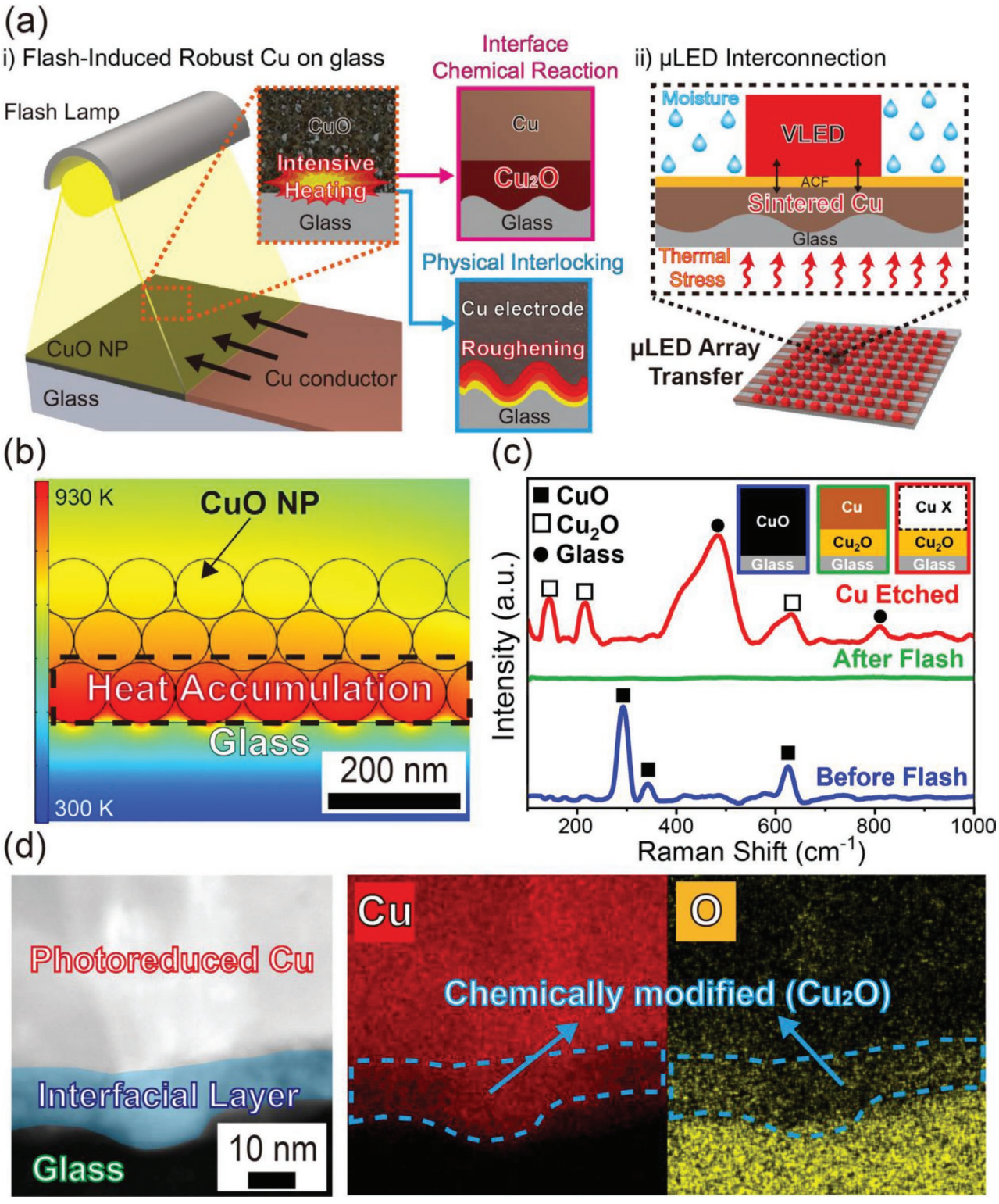

Figure 1. a) Schematic illustration of the flash-induced robust Cu electrode on a glass substrate and its thin-film µLED interconnection. i) Highly robust Cu conductor formed by interface chemical reaction and physical interlocking, caused by intensive photothermal heating at the CuO/glass boundary. ii) The flash-induced Cu electrode integrated with vertical thin-film µLEDs (VLEDs), enabling thin-film µLED array transfer and stable LED operation. b) Temperature of the CuO nanoparticles on a glass substrate during flash illumination, simulated by finite element analysis (FEA). c) Raman spectroscopy of the pristine CuO film (before flash), flash-treated Cu conductor (after flash), and residual Cu_2O film after flash-induced Cu removal (Cu etched). d) Cross-sectional scanning transmission electronic microscopy (STEM) and energy-dispersive X-ray spectroscopy (EDS) mapping of the flash-induced Cu electrode on a glass substrate (Cu: copper; O: oxygen).

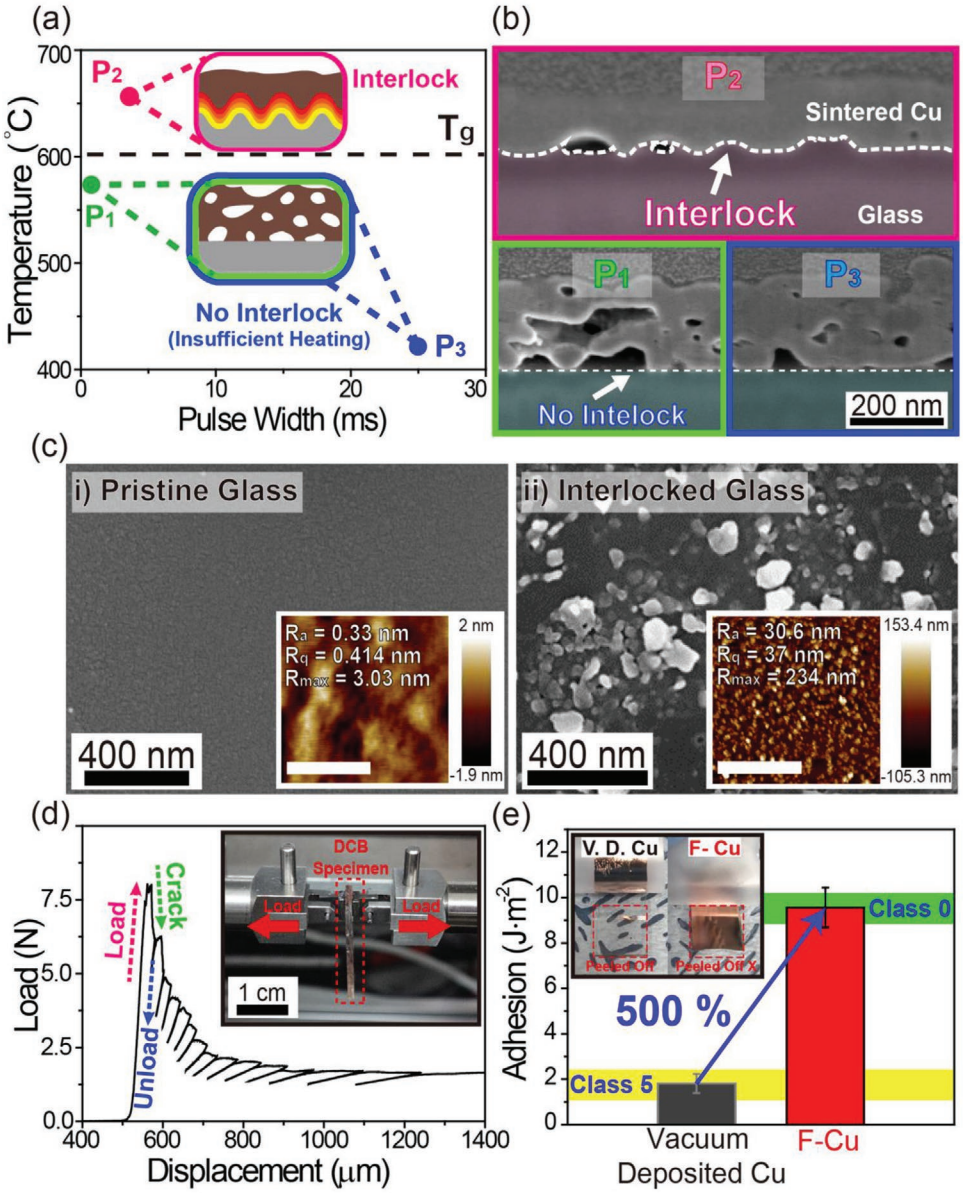

Figure 2. a) FEA-calculated temperature of the CuO/glass interface ($T_{CuO/glass}$) at different processing conditions with pulse widths of 0.66, 3.6, and 25 ms (P_1, P_2, and P_3, respectively). b) Cross-sectional SEM images of the flash-induced Cu electrodes processed by the photothermal treatment of P_1, P_2, and P_3 corresponding to (a). c) Top-view SEM images of the pristine glass (i) and interlocked glass (ii), respectively. The insets show the AFM measurement results of the specimens; scale bar = 5 μm. d) Double-cantilever-beam (DCB) peel test results of the flash-treated Cu electrode, at a constant displacement rate of 0.1 mm s^{-1}. The inset shows a photograph of the DCB specimen bonded to the Al beams for delamination force measurements. e) Adhesion energy of a vacuum-deposited Cu film (VD-Cu) and the flash-induced Cu conductor (F-Cu) based on DCB delamination force measurements. The inset shows the 3M tape peel test of VD-Cu and F-Cu, respectively.

formed at the Cu/glass interface.[64–67] This Cu_2O layer could be induced via re-oxidation of the Cu conductor due to the interfacial photothermal heating,[59,68–70] alleviating the atomic mismatch between flash-induced Cu and glass for highly robust Cu electrode.[71–74] Figure 1d presents the cross-sectional image of flash-activated Cu on a glass substrate, as analyzed by STEM and energy dispersive X-ray spectroscopy (EDS) mapping. The interfacial layer, presented as the blue colored area, had 10 nm thickness and was homogeneously formed between the photoreduced Cu film and substrate. The EDS mapping of flash-activated Cu conductor showed distinct signals of copper and oxygen in the interlayer, confirming the existence of Cu_2O after the photothermal treatment.

Figure 2a shows the numerically (FEA) calculated temperature of CuO/glass interface ($T_{CuO/glass}$) at different processing conditions with pulse widths of 0.66, 3.6, and 25 ms (P_1, P_2, and P_3, respectively) to study the physical interlocking. Energy densities of 7.31, 14.45, and 39.65 J cm^{-2} were inserted into P_1, P_2, and P_3, respectively, based on experimental data for the conductive Cu (Figure S1, Supporting Information). The flash

light under P_2 condition could increase $T_{CuO/glass}$ above the glass transition temperature ($T_g \approx 600$ °C), providing sufficient thermal energy for glass softening.[75–77] Physically softened boundary between the Cu and glass could cause subsequent fluctuation and instantaneous solidification, resulting in the interlocking of Cu/glass interface. On the other hand, the flash light processing of P_1 and P_3 could not form an interlocked interface because the heat was insufficient to modify glass substrates. Note that P_1 with an energy density higher than 7.31 J cm^{-2} induced electrode ablation via nanoparticle vaporization, whereas P_3 with a flash energy above 39.65 J cm^{-2} led to serious Cu oxidation, due to the long time annealing. Figure 2b shows cross-section SEM images of the Cu electrodes fabricated with the P_1, P_2, and P_3 conditions, corresponding to Figure 2a. After the P_2 treatment, the sintered Cu and glass exhibited the interlocked interface with wavy structure. The resulting interlocked interface could significantly increase the Cu/glass contact area to enhance the interfacial fracture energy, adhesion, scratch resistance, and lifetime of Cu conductor.[50] On the other hand, the Cu/glass interface caused by flash light processing with P_1 and P_3 showed no interlocked structure, which was closely related to the glass transition temperature. Figure 2c shows top-view SEM images of pristine glass and interlocked glass to directly observe the substrate morphology changed by flash light processing. The pristine glass substrate showed a clean surface with low average roughness (R_a), root-mean-square roughness (R_q), and maximum roughness (R_{max}) of 0.33, 0.414, and 3.03 nm, respectively, as shown in Figure 2c-i. The flash-processed NPs were welded each other to expand current path, resulting in wavy structure of the Cu electrode as presented in Figure S2 (Supporting Information). Figure 2c-ii presents the rough morphology of interlocked glass surface after removing the flash-activated Cu electrode. The photothermally treated specimen exhibited significantly high R_a, R_q, and R_{max} (30.6, 37, and 234 nm, respectively) compared with the roughness values of pristine sample. These results confirmed that the interface-limited photothermal heating successfully induced the nanoscale interlocking between Cu and glass substrate. Figure 2d shows the fracture force measurement of flash-induced Cu conductor on a glass substrate. The measurement was performed by a DCB peel test and high-accuracy micromechanical equipment. Al beams were bonded to the side of a glass substrate and a Cu electrode by an epoxy adhesive. The ends of Al beams were repetitively loaded and unloaded at a constant displacement rate of 0.1 mm s^{-1} while the applied load was monitored as a function of the displacement. In the initial stage, the DCB specimen was elastically loaded without severe breakage, but as the load increased to 8 N, the Cu conductor started to delaminate from the glass. The load-versus-displacement curve showed a consistent decrease after the applied load reached the critical point of 8 N, indicating successive crack propagation within the Cu/glass interface. Multiple cycles of loading, crack growth, and unloading were performed on the specimen to obtain the experimental values required to calculate the adhesion strength between the Cu electrode and the glass substrate. Figure 2e presents the adhesion energy of flash-processed Cu conductor (F-Cu) and vacuum-deposited Cu thin film (VD-Cu) on a glass substrate based on the DCB peeling force measurements. The adhesion energy of flash-exposed electrode was 10 J m^{-2}, exhibiting 500% higher adhesion force than that of vacuum sputtered Cu. Furthermore, the flash-processed electrode was not delaminated by 3M tape, while the vacuum-deposited metal film was completely peeled off by the same tape, as presented in the inset of Figure 2e. This outstanding robustness of flash-processed Cu conductor could be attributed to the photochemically induced ultrathin Cu_2O interlayer and physically interlocked structure at the Cu/glass interface.

Figure 3a illustrates a layer-by-layer schematic of AlGaInP VLEDs integrated with a flash-induced robust Cu on a glass substrate. The flash-induced Cu film was patterned in a linear shape with a minimum width of 80 µm by selective etching process, as depicted in Figure S3 (Supporting Information). The AlGaInP vertical µLED chips were transferred from a mother GaAs wafer to the Cu pattern lines via ACF bonding process. The LED chips were passivated with SU-8 epoxy of 10 µm thickness to prevent device contamination, followed by the top metal deposition. The electrical interconnection of flash-induced Cu and LED chips was formed by conductive Au/Ni particles in ACF under a heat of 190 °C and high pressure of 3.5 MPa.

Figure 3b compares the optical power density of VLEDs integrated with the robust Cu conductor and vacuum-deposited Cu electrode on glass substrates, as a function of input current density. Excellent output power of the thin-film µLED was achieved in proportional to the injection current without serious thermal degradation, resulted from the outstanding heat sink of flash-induced bottom Cu electrode. As presented in the inset of Figure 3b, the µLED on flash-processed Cu exhibited strong illumination with an optical power density of 41 mW mm^{-2}, which was 35% higher than that of the LED on vacuum-deposited Cu at the current density of 1200 mA mm^{-2}. In addition, the AlGaInP LED with flash-sintered Cu electrode had a forward voltage of ≈3.8 V, and was successfully operated by a wireless power supply system (Figure S4, Supporting Information). This excellent electrical/optical performance of AlGaInP VLED could be explained by the fact that the flash-induced Cu conductor formed a robust interconnection with the VLED in spite of severe thermo-compression. Figure 3c shows the electroluminescence (EL) spectrum of VLEDs based on the flash-activated Cu and vacuum-deposited Cu. Both optoelectronic devices emitted a light with peak wavelength of 632.13 nm, representing that the thin-film µLEDs were fabricated by same epitaxial wafer and packaging process. The CIE coordinates of AlGaInP LED on the flash-processed Cu electrode were (0.6956, 0.3022), representing high hue of red light, as described in the inset of Figure 3c.

Figure 4a schematically illustrates the possible degradation mechanism of VLED on the flash-induced Cu electrode under environmental stresses of temperature and humidity. When moisture infiltrates the VLED through a vulnerable Cu/glass interface, the electrode can be deteriorated by corrosion, oxidation, and breakage of the Cu, interfering with the stable current injection into the thin-film µLED. In addition, significant tensile stress can be applied in the Cu layer due to the thermal expansion mismatch between Cu and glass substrates during ambient heating, which causes serious performance degradation of the thin-film µLED via electrode delamination. The reliability of VLED with the flash-induced Cu conductor was experimentally

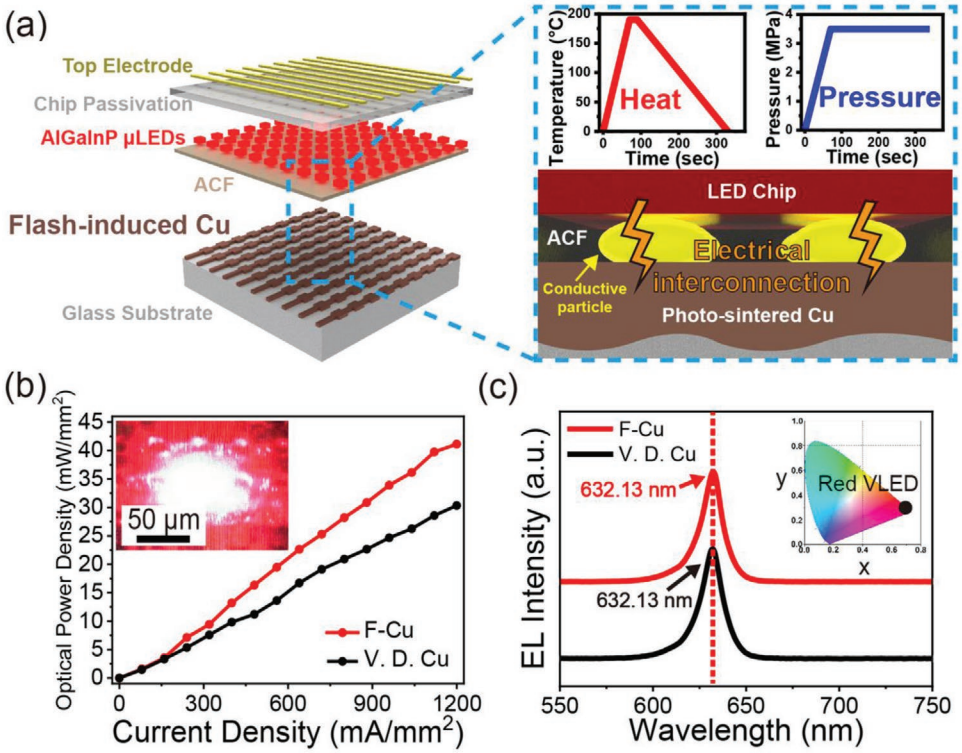

Figure 3. a) Schematic illustrations of AlGaInP vertical thin-film μLEDs (VLEDs) integrated with the flash-induced Cu conductor, and electrical interconnection between the flash-activated Cu and LED via conductive particles in the thermo-compressed anisotropic conductive film (ACF). b) Optical power density of the VLEDs on flash-processed Cu conductor (red) and vacuum-deposited Cu electrode (black) as a function of the injection current density. The inset shows an optical microscopy image of the red light illuminating VLED fabricated with the flash-induced Cu electrode. c) Electroluminescence (EL) spectrum of the VLEDs on flash-activated Cu electrode (red) and vacuum-deposited Cu conductor (black). The inset presents the CIE color coordinates of red light emitted from the VLED with flash-processed Cu.

compared with that of LED on vacuum-deposited Cu film via environmental examinations such as high-temperature storage test, temperature humidity test, and thermal shock test. Figure 4b presents the forward voltage change and normalized optical power of VLED integrated with the flash-induced Cu conductor during the high-temperature storage test. The μLED exhibited negligible changes in optical power and forward voltage in spite of the intensive heating of 100 °C for 48 h; this was attributed to the outstanding adhesion strength of Cu that prevented electrode delamination from the substrates. For the LED on vacuum-deposited Cu film, output power degradation and severe forward voltage increase were observed during the same reliability test, as described in Figure S5 (Supporting Information). Figure 4c shows the electrical/optical performance of VLEDs on the flash-processed Cu and vacuum-deposited Cu during temperature humidity storage tests, in 85 °C/85% relative humidity. The AlGaInP LED on flash-induced Cu electrode maintained its initial voltage despite the 48 h of storage in a hot and humid environment, while the LED integrated with vacuum-deposited Cu exhibited a drastic forward voltage increase after 6 h of testing. Furthermore, the flash-processed Cu enabled superior VLED stability compared to the vacuum-deposited Cu from the perspective of output power, as presented in the inset of Figure 4c. This reliable VLED performance could be demonstrated by the significant robustness of flash-activated Cu conductor, suppressing electrode deterioration due to moisture infiltration. Figure 4d shows the normalized optical power and forward voltage variation of VLED on the Cu conductor during the thermal shock test. The AlGaInP LED exhibited consistent operation despite the 150 cycles of harsh temperature change. The LED fabricated by vacuum-deposited copper, however, had severe performance degradation caused by 100 thermal shocks, as depicted in Figure S6 (Supporting Information).

To verify the robust flash-processed Cu conductor, 50 × 50 AlGaInP thin-film VLED arrays were transferred and interconnected to patterned Cu electrodes on a display substrate of corning glass in one time. **Figure 5**a shows the forward voltage (V_f) measurement of VLEDs on flash-induced Cu electrodes. The electrical property of each LED was measured by a parameter analyzer (Keithley 4200-SCS). Based on Ohm's law, the V_f of VLED could be expressed as equation (2)[78,79]

$$V_f = I_{dc} \cdot \left(R_{F-Cu} + R_{ACF} + R_{Chip}\right) \quad (2)$$

where V_f is the forward voltage of VLED, I_{dc} is the DC current injected into the VLED, $R_{F\text{-}Cu}$ is the electrical resistance of flash-activated Cu conductor, R_{ACF} is the electrical resistance of ACF, and R_{Chip} is the electrical resistance of LED chip, respectively (left inset of Figure 5a). R_{ACF} and R_{Chip} of VLED had similar values because the LED arrays were made from the same ACF and epitaxial wafers. Therefore, the V_f difference among VLEDs

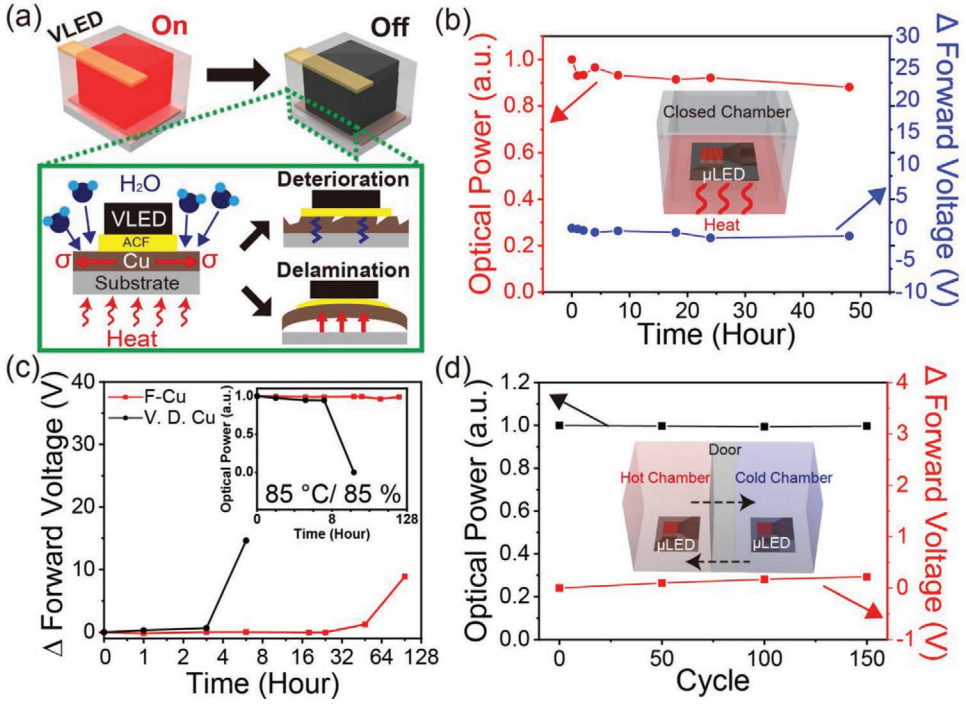

Figure 4. a) Schematic illustration of possible breakdown mechanism of the VLED on flash-induced Cu electrode under thermal stress and moisture infiltration. b) Normalized optical power and forward voltage change of the VLED on flash-induced Cu electrode during the high-temperature storage test (T = 100 °C, I = 1 mA). c) Forward voltage change in the VLEDs on flash-induced Cu (red) and vacuum-deposited Cu (black) during temperature humidity storage test (RH = 85%, T = 85 °C, I = 500 μA). The inset shows the normalized optical power of VLEDs on the vacuum-deposited Cu (black) and flash-processed Cu (red) during the temperature humidity storage testing. d) Normalized optical power and forward voltage change of the VLED on flash-induced Cu electrode during thermal shock test (T_{high} = 110 °C, T_{low} = −40 °C, t_{dwell} = 15 min, I = 1 mA).

would be determined by the $R_{F\text{-}Cu}$ of VLED at constant DC current. As presented in the right inset of Figure 5a, 10 × 10 sub VLED arrays selected from the 50 × 50 LEDs displayed no significant difference in V_f (except for four dead pixels) at 1 mA current injection due to the uniform electrical resistance of flash-induced Cu electrodes. Figure 5b presents the temperature distribution of 50 × 50 VLED arrays under a constant current injection of 30 mA. To measure the temperature of μLEDs, the overall light emitting region was divided into 10 partial areas consisting of 5 × 50 pixels, as illustrated in the left inset of Figure 5b. The VLED temperature changed within 1.5 °C in each LED area, while the median temperature of 10 LED areas ranged from 25 to 26 °C. The thin-film μLEDs exhibited a consistent temperature of around 27 °C regardless of operating time, as presented in the right inset of Figure 5b. Note that the flash-induced Cu uniformly dissipated the heat generated by the VLEDs without severe electrode damage owing to high Cu/glass adhesion. Figure 5c shows the luminance distribution of AlGaInP VLED arrays measured at 35 mA injection current. The average output power of μLEDs was 331 cd m^{-2} under absolute dark condition, which was comparable to the optical performance of a commercial smart-phone display panel.[80] The 7 × 7 mm^2 sized light-emitting area had little dark spots, indicating the high transfer yield of thin-film μLEDs on the robust flash-induced Cu electrodes, as shown in the inset of Figure 5c. The inset of Figure 5d shows the pure red light illumination of 50 × 50 VLED arrays on the flash-induced Cu electrodes at 30 mA injection current. Figure 5d displays the wavelengths of 200 LEDs among the 50 × 50 VLEDs, indicating uniform distribution with a prominent peak wavelength of 623.3 nm and a standard deviation of 0.224 nm (Figure S7, Supporting Information). These high production yields and uniform optical performance of VLED arrays demonstrated the remarkable compatibility of flash-induced Cu electrodes for thin-film μLED displays.

In summary, we developed a robust flash-induced Cu electrode on a glass display substrate for μLEDs via chemical and physical interlocking between the Cu and glass. During one shot of 3.6 ms flash illumination, CuO NPs on a glass substrate were transformed into a Cu conductor by chemical reduction and sintering. Simultaneously, the photothermal heat accumulated at the boundary of CuO and glass, forming a 10 nm thick Cu_2O interlayer between photoreduced Cu and glass, to resolve inherent atomic mismatch. A flash light with a pulse width of 3.6 ms and energy density of 14.45 J cm^{-2} softened the glass substrate and caused Cu nanointerlocking, increasing the Cu/glass contact area and interfacial fracture energy. Electrode adhesion enhancement of the flash-induced interface interactions was verified by comparing the adhesion energy of flash-activated Cu (10 J m^{-2}) and vacuum-deposited Cu (2 J m^{-2}) via DCB peel test. The AlGaInP VLED formed a robust interconnection with flash-induced Cu electrode despite of harsh ACF bonding conditions (190 °C heat and 3.5 MPa pressure), resulting in a high output power of 41 mW mm^{-2} and a peak wavelength of red light with 626.32 nm. The VLED on flash-processed Cu conductor presented consistent forward voltage

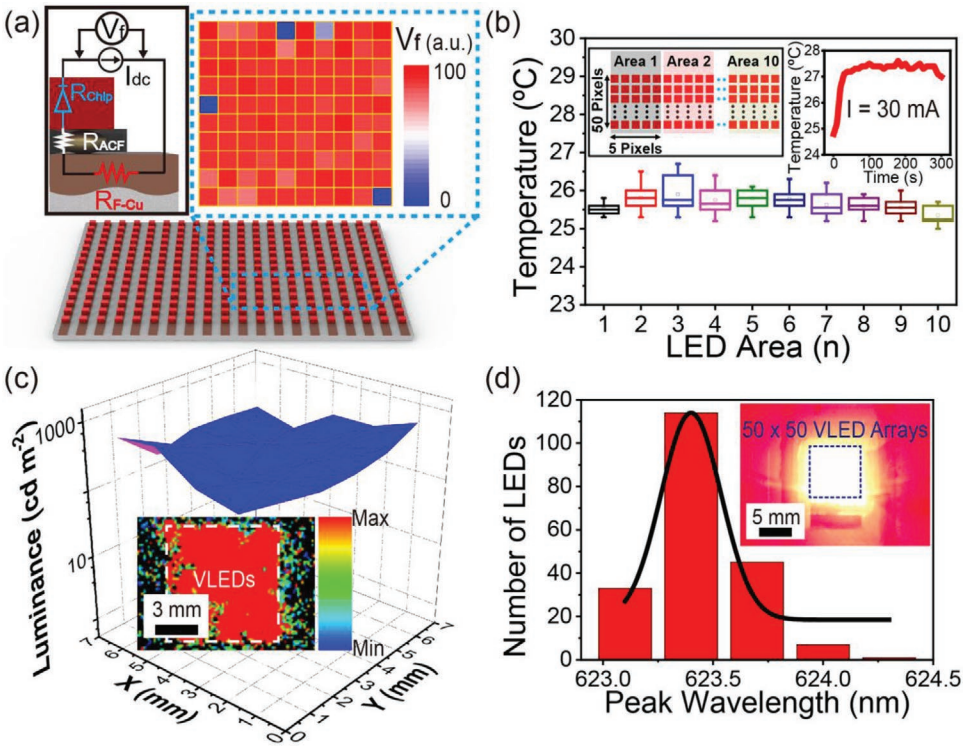

Figure 5. a) Normalized forward voltage (V_f) of 10 × 10 LEDs among 50 × 50 VLED arrays on flash-induced Cu electrode at an injection current of 1 mA. The left inset schematically describes the V_f measurement of VLED and the parameters that determined the V_f of VLED. b) Temperature distribution of the 50 × 50 VLEDs at an injection current of 30 mA. The inset shows a schematic illustration of the LED area consisting of 5 × 50 pixels (left) and temperature measurements of the VLED arrays during 300 s of operation (right, I = 30 mA). c) Luminance distribution of 50 × 50 VLED arrays on the flash-treated Cu electrode (I = 35 mA). The inset shows a pseudocolor luminance image of VLEDs. Colored spots in the image indicate the light emitted by the VLEDs. d) Peak wavelength of 200 LEDs among 50 × 50 VLED arrays on the flash-activated Cu electrode. The inset shows a photograph of the VLED arrays illuminating pure red light.

and optical power even after 48 h of intensive heating (100 °C), 48 h of moisture infiltration (85 °C/85% RH), and 150 cycles of thermal stress (–40 °C/110 °C). The 50 × 50 VLED arrays on flash-activated Cu electrode exhibited high transfer yield, similar forward voltage, small temperature change within 1.5 °C, and uniform wavelength distribution with a standard deviation of 0.224 nm. Flash-based Cu interconnection technology can be an important tool for fabricating low-cost μLED displays.

Experimental Section

Flash-Induced Cu Fabrication: A CuO nanoparticle ink (NovaCentrix Corp.) was spin-coated onto a glass substrate at 2000 rpm and dried in 60 °C oven for 2 h. A flash light illuminated the CuO nanoparticles on the glass substrates to induce photochemical reduction and sintering, resulting in the formation of flash-induced Cu electrode. To optimize the electrical resistivity of Cu electrode, the CuO NPs were treated by flash light with different pulse widths and energy densities, as shown in Figure S1 (Supporting Information).

Characterizations: Cross-sectional morphologies of the flash-induced Cu electrode and the CuO nanoparticles were observed by means of FIB-SEM (Helios Nanolab 450 F1, FEI) and TEM (Talos F200X, FEI) in Kaist Analysis Center for Research Advancement (KARA). The elemental compositions of the photoreduced Cu conductor and the CuO nanoparticles were monitored by EDS (Talos F200X, FEI). The Raman spectroscopy of the pristine CuO, photosintered Cu, and the residual Cu_2O film was performed by the high-resolution Raman system (LabRAM HR Evolution Visible_NIR, HORIBA). The cross-sections of the flash-processed Cu conductor with different flash pulse width were observed by SEM (SU5000, Hitachi).

VLED Fabrication: AlGaInP epitaxial layers grown on n-type GaAs wafer were served as the active material, as shown in Figure S8a (Supporting Information). Figure S8b (Supporting Information) indicates that Cr (10 nm) and Au (50 nm) were deposited as ohmic contact on the LED surface, followed by the chip isolation via inductively coupled plasma reactive ion etching (ICP-RIE). During the 300 s of the dry etching, the pressure was maintained at 10 mTorr under the gas condition of Cl_2 (60 sccm) and Ar (10 sccm), and the plasma was occurred by the bias of 400 W/100 W. As depicted in Figure S8c (Supporting Information), the exposed GaAs wafer was passivated by photoreactive polymer to protect the bottom electrode during GaAs etching. The flash-induced Cu electrode on the glass substrate was pattered by high-resolution photolithography and wet etching, and served as the bottom electrode of the VLED as displayed in Figure S8d (Supporting Information). To prevent the damage of the Cu electrode during GaAs etching, the electrode that was not covered by the LED wafer was protected by the photoreactive polymer. Figure S8e (Supporting Information) presents that the LED chips on the GaAs wafer were interconnected with the flash-induced Cu conductor via the ACF bonding process. As described in Figure S8f (Supporting Information), the GaAs wafer was selectively etched by the solution consisting of the citric acid ($C_6H_8O_7$) and hydrogen peroxide (H_2O_2) (volume ratio of 6:1) at the ambient temperature of 60 °C, followed by removing the polymer for the electrode protection. The LED chips and the bottom electrode were passivated by the photoresist (SU-8 3010) using a conventional photolithography technique. AgNW solution (Nanopyxis Corp.) was spin-coated at 1500 rpm on the passivation layer followed by solvent drying, and Cu (100 nm) was deposited by e-beam

evaporator. Both conductors were patterned to form top electrode of the VLED, as represented in Figure S8g (Supporting Information). Figure S8h (Supporting Information) displays that the photoresist (SU-8 3005) covered the entire VLED except the end of the electrodes for the device encapsulation.

VLED Performance Measurements: The EL spectrum, peak wavelength, and optical power of the VLEDs were measured by optical spectroscopy (AvaSpec-UIS2048-RS, Avantes Corp.). The *I–V* characteristic of the VLED was measured by a semiconductor characterization system (Keithley 4200-SCS) with current sweep mode. The forward voltage of the VLED arrays was analyzed using the same equipment under the constant DC current of 1 mA. The luminescence of the VLEDs was investigated by 2D color analyzer under the injection current of 35 mA. The temperature of the VLED arrays was measured by the thermometer with the thermocouple under the injection current of 30 mA.

Reliability Tests of the VLEDs: The high-temperature storage test was conducted by the mechanical convection oven (Myoungsung Engineering Corp.) under the ambient temperature of 100 °C. For temperature humidity test, the VLEDs were placed in the temperature humidity chamber under the condition of 85 °C/85% RH. During one thermal shock cycle, the VLEDs were alternately placed in hot chamber (110 °C) and cold chamber (–40 °C) with the dwell time of 15 min. The electrical/optical properties of the LEDs were measured after every 50 thermal shock cycle.

Supporting Information

Supporting Information is available from the Wiley Online Library or from the author.

Acknowledgements

J.H.S. and J.H.P. contributed equally to this work. This work was supported by Nano-Material Technology Development Program (NRF-2016M3A7B4910636), Wearable Platform Materials Technology Center (WMC) (NRF-2016R1A5A1009926), and Convergent Technology R&D Program for Human Augmentation (NRF-2020M3C1B8081519) through the National Research Foundation of Korea (NRF) funded by the Ministry of Science, ICT and Future Planning.

Conflict of Interest

The authors declare no conflict of interest.

Data Availability Statement

Research data are not shared.

Keywords

Cu electrodes, glass, interface chemistry, physical interlocking, thin-film μLEDs

Received: October 21, 2020
Revised: December 18, 2020
Published online: February 26, 2021

[1] H. E. Lee, J. H. Shin, J. H. Park, S. K. Hong, S. H. Park, S. H. Lee, J. H. Lee, I.-S. Kang, K. J. Lee, *Adv. Funct. Mater.* **2019**, *29*, 1808075.
[2] H. E. Lee, J. Choi, S. H. Lee, M. Jeong, J. H. Shin, D. J. Joe, D. Kim, C. W. Kim, J. H. Park, J. H. Lee, D. Kim, C.-S. Shin, K. J. Lee, *Adv. Mater.* **2018**, *30*, 1800649.
[3] S.-I. Park, Y. Xiong, R.-H. Kim, P. Elvikis, M. Meitl, D.-H. Kim, J. Wu, J. Yoon, C.-J. Yu, Z. Liu, Y. Huang, K.-c. Hwang, P. Ferreira, X. Li, K. Choquette, J. A. Rogers, *Science* **2009**, *325*, 977.
[4] R.-H. Kim, D.-H. Kim, J. Xiao, B. H. Kim, S.-I. Park, B. Panilaitis, R. Ghaffari, J. Yao, M. Li, Z. Liu, V. Malyarchuk, D. G. Kim, A.-P. Le, R. G. Nuzzo, D. L. Kaplan, F. G. Omenetto, Y. Huang, Z. Kang, J. A. Rogers, *Nat. Mater.* **2010**, *9*, 929.
[5] L. Tan, Q. Zhou, H. Wang, R. Yao, *IEEE Photonics Technol. Lett.* **2019**, *31*, 1705.
[6] H. Q. T. Bui, R. T. Velpula, B. Jain, O. H. Aref, H.-D. Nguyen, T. R. Lenka, H. P. T. Nguyen, *Micromachines* **2019**, *10*, 492.
[7] X. Li, L. Wu, Z. Liu, B. Hussain, W. C. Chong, K. M. Lau, C. P. Yue, *J. Lightwave Technol.* **2016**, *34*, 3449.
[8] M. A. Meitl, Z.-T. Zhu, V. Kumar, K. J. Lee, X. Feng, Y. Y. Huang, I. Adesida, R. G. Nuzzo, J. A. Rogers, *Nat. Mater.* **2006**, *5*, 33.
[9] D. H. Kim, H. G. Yoo, S. M. Hong, B. Jang, D. Y. Park, D. J. Joe, J.-H. Kim, K. J. Lee, *Adv. Mater.* **2016**, *28*, 8371.
[10] S. H. Lee, J. Kim, J. H. Shin, H. E. Lee, I.-S. Kang, K. Gwak, D.-S. Kim, D. Kim, K. J. Lee, *Nano Energy* **2018**, *44*, 447.
[11] A. Paranjpe, J. Montgomery, S. M. Lee, S. I. D. Symp, *Dig. Tech. Pap.* **2019**, *50*, 169.
[12] Y.-C. Jeong, H. E. Lee, A. Shin, D.-G. Kim, K. J. Lee, D. Kim, *Adv. Mater.* **2020**, *32*, 1907522.
[13] R.-H. Kim, M.-H. Bae, D. G. Kim, H. Cheng, B. H. Kim, D.-H. Kim, M. Li, J. Wu, F. Du, H.-S. Kim, S. Kim, D. Estrada, S. W. Hong, Y. Huang, E. Pop, J. A. Rogers, *Nano Lett.* **2011**, *11*, 3881.
[14] A. H. Park, S. H. Lee, C. Lee, J. Kim, H. E. Lee, S.-B. Paik, K. J. Lee, D. Kim, *ACS Nano* **2016**, *10*, 2791.
[15] C. K. Jeong, K.-I. Park, J. H. Son, G.-T. Hwang, S. H. Lee, D. Y. Park, H. E. Lee, H. K. Lee, M. Byun, K. J. Lee, *Energy Environ. Sci.* **2014**, *7*, 4035.
[16] K. R. Son, B. R. Lee, T. G. Kim, *ACS Appl. Mater. Interfaces* **2018**, *10*, 40967.
[17] V. R. Marinov, S. I. D. Symp, *Dig. Tech. Pap.* **2018**, *49*, 692.
[18] R. Bao, C. Wang, L. Dong, R. Yu, K. Zhao, Z. L. Wang, C. Pan, *Adv. Funct. Mater.* **2015**, *25*, 2884.
[19] Y. Peng, M. Que, H. E. Lee, R. Bao, X. Wang, J. Lu, Z. Yuan, X. Li, J. Tao, J. Sun, J. Zhai, K. J. Lee, C. Pan, *Nano Energy* **2019**, *58*, 633.
[20] Y. Chen, K. Denis, P. Kazlas, P. Drzaic, S. I. D. Symp, *Dig. Tech. Pap.* **2001**, *32*, 157.
[21] C.-J. Lee, D.-G. Moon, J.-I. Han, S. I. D. Symp, *Dig. Tech. Pap.* **2004**, *35*, 1005.
[22] U. Shankar, D. Oberoi, S. Avasarala, S. Ali, A. Bandyopadhyay, *J. Mater. Sci.* **2019**, *54*, 6684.
[23] Y. S. Choi, J. U. Yun, S. E. Park, *J. Non-Cryst. Solids* **2016**, *431*, 2.
[24] R. A. Matula, *J. Phys. Chem. Ref. Data* **1979**, *8*, 1147.
[25] D. Edelstein, J. Heidenreich, R. Goldblatt, W. Cote, C. Uzoh, N. Lustig, P. Roper, T. McDevitt, W. Motsiff, A. Simon, J. Dukovic, R. Wachnik, H. Rathore, R. Schulz, L. Su, S. Luce, J. Slattery, in *Int. Electron Devices Meet. IEDM Tech. Dig.,* IEEE, Piscataway, NJ, USA **1997**, pp. 773–776, https://doi.org/10.1109/IEDM.1997.650496.
[26] S. M. Alam, F. L. Wei, C. L. Gan, C. V. Thompson, D. E. Troxel, *Sixth Int. Symp. Qual. Electron. Des.* **2005**, 303.
[27] M. D. Susman, Y. Feldman, A. Vaskevich, I. Rubinstein, *Chem. Mater.* **2012**, *24*, 2501.
[28] J. Peng, K. Lu, S. Hu, Z. Fang, H. Ning, J. Wei, Z. Zhu, Y. Zhou, L. Wang, R. Yao, X. Lu, *Appl. Sci.* **2017**, *7*, 820.
[29] P.-T. Liu, Y.-T. Chou, C.-Y. Su, H.-M. Chen, *Surf. Coat. Technol.* **2010**, *205*, 1497.
[30] C.-Y. Ho, Y.-J. Chang, *Solid-State Electron.* **2016**, *116*, 130.
[31] B.-H. Seo, S.-H. Lee, I.-S. Park, J. H. Seo, H. Choe, J.-H. Jeon, M.-p. Hong, *Curr. Appl. Phys.* **2011**, *11*, S262.
[32] C.-C. Lai, H.-K. Chiu, Y.-P. Lin, Y.-C. Kuan, O. Sun, S. I. D. Symp, *Dig. Tech. Pap.* **2006**, *37*, 1882.
[33] K. H. Jang, W. J. Lee, H. R. Kim, G. Y. Yeom, *Jpn. J. Appl. Phys.* **2004**, *43*, 8300.

[34] B. K. You, W. I. Park, J. M. Kim, K.-I. Park, H. K. Seo, J. Y. Lee, Y. S. Jung, K. J. Lee, *ACS Nano* **2014**, *8*, 9492.
[35] S. H. Sung, Y. S. Kim, D. J. Joe, B. H. Mun, B. K. You, D. H. Keum, S. K. Hahn, M. Berggren, D. Kim, K. J. Lee, *Nano Energy* **2018**, *51*, 102.
[36] J. H. Han, K. M. Bae, S. K. Hong, H. Park, J.-H. Kwak, H. S. Wang, D. J. Joe, J. H. Park, Y. H. Jung, S. Hur, C. D. Yoo, K. J. Lee, *Nano Energy* **2018**, *53*, 658.
[37] R. R. Gattass, E. Mazur, *Nat. Photonics* **2008**, *2*, 219.
[38] E. C. Garnett, W. Cai, J. J. Cha, F. Mahmood, S. T. Connor, M. G. Christoforo, Y. Cui, M. D. McGehee, M. L. Brongersma, *Nat. Mater.* **2012**, *11*, 241.
[39] E. H. Penilla, L. F. Devia-Cruz, A. T. Wieg, P. Martinez-Torres, N. Cuando-Espitia, P. Sellappan, Y. Kodera, G. Aguilar, J. E. Garay, *Science* **2019**, *365*, 803.
[40] Y.-B. Park, B. Min, K. J. Vahala, H. A. Atwater, *Adv. Mater.* **2006**, *18*, 1533.
[41] W. I. Park, B. K. You, B. H. Mun, H. K. Seo, J. Y. Lee, S. Hosaka, Y. Yin, C. A. Ross, K. J. Lee, Y. S. Jung, *ACS Nano* **2013**, *7*, 2651.
[42] H. E. Lee, J. H. Park, T. J. Kim, D. Im, J. H. Shin, D. H. Kim, B. Mohammad, I.-S. Kang, K. J. Lee, *Adv. Funct. Mater.* **2018**, *28*, 1801690.
[43] D. J. Joe, S. Kim, J. H. Park, D. Y. Park, H. E. Lee, T. H. Im, I. Choi, R. S. Ruoff, K. J. Lee, *Adv. Mater.* **2017**, *29*, 1606586.
[44] H. M. Jin, D. Y. Park, S.-J. Jeong, G. Y. Lee, J. Y. Kim, J. H. Mun, S. K. Cha, J. Lim, J. S. Kim, K. H. Kim, K. J. Lee, S. O. Kim, *Adv. Mater.* **2017**, *29*, 1700595.
[45] T. Jeon, H. M. Jin, S. H. Lee, J. M. Lee, H. I. Park, M. K. Kim, K. J. Lee, B. Shin, S. O. Kim, *ACS Nano* **2016**, *10*, 7907.
[46] J. H. Han, J.-H. Kwak, D. J. Joe, S. K. Hong, H. S. Wang, J. H. Park, S. Hur, K. J. Lee, *Nano Energy* **2018**, *53*, 198.
[47] M. Shimizu, K. Miura, M. Sakakura, M. Nishi, Y. Shimotsuma, S. Kanehira, T. Nakaya, K. Hirao, *Appl. Phys. A* **2010**, *100*, 1001.
[48] J. H. Park, H. E. Lee, C. K. Jeong, D. H. Kim, S. K. Hong, K.-I. Park, K. J. Lee, *Nano Energy* **2019**, *56*, 531.
[49] J. H. Park, G.-T. Hwang, S. Kim, J. Seo, H.-J. Park, K. Yu, T.-S. Kim, K. J. Lee, *Adv. Mater.* **2017**, *29*, 1603473.
[50] J. H. Park, S. Han, D. Kim, B. K. You, D. J. Joe, S. Hong, J. Seo, J. Kwon, C. K. Jeong, H.-J. Park, T.-S. Kim, S. H. Ko, K. J. Lee, *Adv. Funct. Mater.* **2017**, *27*, 1701138.
[51] I. Choi, H. Y. Jeong, H. Shin, G. Kang, M. Byun, H. Kim, A. M. Chitu, J. S. Im, R. S. Ruoff, S.-Y. Choi, K. J. Lee, *Nat. Commun.* **2016**, *7*, 13562.
[52] I. Choi, H. Y. Jeong, D. Y. Jung, M. Byun, C.-G. Choi, B. H. Hong, S.-Y. Choi, K. J. Lee, *ACS Nano* **2014**, *8*, 7671.
[53] D. Angmo, T. T. Larsen-Olsen, M. Jørgensen, R. R. Søndergaard, F. C. Krebs, *Adv. Energy Mater.* **2013**, *3*, 172.
[54] J. H. Park, J. Seo, C. Kim, D. J. Joe, H. E. Lee, T. H. Im, J. Y. Seok, C. K. Jeong, B. S. Ma, H. K. Park, T.-S. Kim, K. J. Lee, *Adv. Sci.* **2018**, *5*, 1801146.
[55] Z. Wang, J. E. Alaniz, W. Jang, J. E. Garay, C. Dames, *Nano Lett.* **2011**, *11*, 2206.
[56] D. H. Jung, J. H. Park, H. E. Lee, J. Byun, T. H. Im, G. Y. Lee, J. Y. Seok, T. Yun, K. J. Lee, S. O. Kim, *Nano Energy* **2019**, *61*, 236.
[57] J. Fukai, M. Kanou, Y. Kodama, O. Miyatake, *Energy Convers. Manage.* **2000**, *41*, 1543.
[58] H. D. Young, F. W. Sears, *University Physics*, Addison-Wesley, Boston, MA, USA **1992**.
[59] M. Mizoshiri, Y. Ito, S. Arakane, J. Sakurai, S. Hata, *Jpn. J. Appl. Phys.* **2016**, *55*, 06GP05.
[60] A. B. Bodade, M. A. Taiwade, G. N. Chaudhari, *J. Appl. Pharm. Res.* **2017**, *5*, 30.
[61] M. Rashad, M. Rüsing, G. Berth, K. Lischka, A. Pawlis, *J. Nanomater.* **2013**, *2013*, 714853.
[62] S. H. Kim, N. Bazin, J. I. Shaw, J.-H. Yoo, M. A. Worsley, J. H. Satcher, J. D. Sain, J. D. Kuntz, S. O. Kucheyev, T. F. Baumann, A. V. Hamza, *ACS Appl. Mater. Interfaces* **2016**, *8*, 34706.
[63] I. R. Lewis, *Handbook of Raman Spectroscopy*, CRC Press, Boca Raton, FL, USA **2001**.
[64] A. Anu, M. A. Khadar, *AIP Adv.* **2015**, *5*, 097176.
[65] E. Kecsenovity, B. Endrődi, Z.s. Pápa, K. Hernádi, K. Rajeshwar, C. Janáky, *J. Mater. Chem. A* **2016**, *4*, 3139.
[66] X. Liu, M. Xu, J. Ma, X. Zhang, C. Luan, X. Feng, A. Song, *Ceram. Int.* **2017**, *43*, 15500.
[67] Y. Liu, F. Ren, S. Shen, Y. Fu, C. Chen, C. Liu, Z. Xing, D. Liu, X. Xiao, W. Wu, X. Zheng, Y. Liu, C. Jiang, *Appl. Phys. Lett.* **2015**, *106*, 123901.
[68] M. Mizoshiri, Y. Ito, J. Sakurai, S. Hata, *Proc. SPIE* **2017**, *10167*, 101671G.
[69] B. Kang, S. Han, J. Kim, S. Ko, M. Yang, *J. Phys. Chem. C* **2011**, *115*, 23664.
[70] M. Mizoshiri, S. Hata, *Res. Rev. J. Mater. Sci.* **2016**, *4*, 47.
[71] H. Nagai, T. Suzuki, H. Hara, C. Mochizuki, I. Takano, T. Honda, M. Sato, *Mater. Chem. Phys.* **2012**, *137*, 252.
[72] X. Li, H. Gao, C. J. Murphy, L. Gou, *Nano Lett.* **2004**, *4*, 1903.
[73] M. Ristov, G. J. Sinadinovski, I. Grozdanov, *Thin Solid Films* **1985**, *123*, 63.
[74] S. Mori, A. Kawai, *Jpn. J. Appl. Phys.* **2010**, *49*, 075804.
[75] T. Uno, T. Kasuga, S. Nakayama, A. J. Ikushima, *J. Am. Ceram. Soc.* **1993**, *76*, 539.
[76] A. Iles, A. Oki, N. Pamme, *Microfluid. Nanofluid.* **2007**, *3*, 119.
[77] A. Stalmashonak, A. Podlipensky, G. Seifert, H. Graener, *Appl. Phys. B: Lasers Opt.* **2009**, *94*, 459.
[78] L. Wang, Y. Zhang, X. Li, Z. Liu, E. Guo, X. Yi, J. Wang, H. Zhu, G. Wang, *J. Phys. D: Appl. Phys.* **2012**, *45*, 505102.
[79] D. K. Ferry, *Science* **2012**, *335*, 45.
[80] R. M. Soneira, *Inf. Disp.* **2013**, *29*, 12.

